Surface & Coatings Technology 223 (2013) 41–46

Contents lists available at SciVerse ScienceDirect

Surface & Coatings Technology

journal homepage: www.elsevier.com/locate/surfcoat

Microstructure and corrosion behavior of AISI 316L duplex treated by means of ion nitriding and plasma based ion implantation and deposition

L. Escalada [a], J. Lutz [b], S.P. Brühl [c], M. Fazio [d], A. Márquez [d], S. Mändl [b], D. Manova [b], S.N. Simison [a],*

[a] Corrosion Division, INTEMA, Faculty of Engineering, University of Mar del Plata, Juan B. Justo 4302, Mar del Plata, Argentina
[b] Leibniz Institute of Surface Modification (IOM), Permoserstr., 15, 04318 Leipzig, Germany
[c] Surface Engineering Group, Universidad Tecnológica Nacional (UTN-FRCU), Ing. Pereira 676, E3264BTD Concepción del Uruguay, Argentina
[d] INFIP (CONICET-University of Buenos Aires), Ciudad Universitaria, Pab. 1, 1428 Ciudad de Buenos Aires, Argentina

ARTICLE INFO

Article history:
Received 9 April 2012
Accepted in revised form 13 February 2013
Available online 5 March 2013

Keywords:
Plasma nitriding
TiN coating
Plasma ion implantation
Corrosion resistance

ABSTRACT

Austenitic stainless steels are the preferred materials for mechanical components in the food, oil and chemical industries due to their good corrosion resistance but they often suffer severe wear due to their poor tribological properties. Plasma surface engineering has been extended to stainless steel hardening, through the modification of the surface with ion nitriding or the application of hard coatings.

In this work, AISI 316L samples were coated with titanium nitride by means of a cathodic arc (CA) and this technique was combined with plasma immersion ion implantation, in a process called plasma based ion implantation and deposition (PBII&D). The effect on corrosion resistance was analyzed, also considering ion nitriding as a pre-treatment. Microstructure and composition were analyzed by means of glancing angle XRD, SIMS, SEM, SEM-FIB and EDS. Localized corrosion resistance was analyzed in a cyclic potentiodynamic polarization experiment in 3.5% NaCl solution, and the corroded surface was analyzed with AFM, SEM and EDS as well. It was found that nitriding at 400 °C produces a thin nitrided layer with good corrosion resistance. A duplex TiN coating resulted in a further improvement of the corrosion resistance. Comparing cathodic arc and PBII&D coating techniques, the last one gives the thickest film and also the best corrosion behavior with good adhesion.

1. Introduction

AISI 316L stainless steel is widely used in components of the oil and gas, food and beverage and chemical industries, as well as a biomaterial due to its outstanding corrosion resistance in aggressive environments. On the other side, all austenitic stainless steels have poor tribological properties, and components should often be replaced because of wear degradation.

In recent years many surface treatments like nitriding and coatings have been investigated with promising results, and many of them are plasma assisted processes. For example, low temperature nitriding can be successfully applied to stainless steel and corrosion resistance is retained if nitride formation is avoided, and a pure "S" phase is obtained, normally at process temperatures of 350–400 °C [1–8]. However at this low temperature only a thin layer of 1–5 μm can be attained with a hardness of between 1000–1500 HV. A higher hardness can be reached applying a thin ceramic coating such as TiN. Several techniques were reported for depositing TiN over steel, such as cathodic arc, magnetron sputtering or ion plating, and plasma CVD. Wear resistance is improved because the coating has a high hardness and a low friction coefficient [9–11]. Even better mechanical properties can be obtained with a duplex process: for instance TiN on a nitrided surface, which enhances the fracture resistance of a hard and brittle coating on top of a ductile and soft substrate. However, adhesion of hard coatings over steel or nitrided steels (duplex treatment) is still a problem [12–14], and other interlayers or combined treatments are being studied at the moment [15–18]. A bad adhesion can lead not only to mechanical failure but also to crevice corrosion attack.

Cathodic arc (CA) processes are well known for the high deposition rate and the possibility to provide coatings with a high hardness. When deposition is combined with implantation, using a high pulse voltage bias on the sample, intermixing can be achieved and the process is known as Plasma based Ion Implantation & Deposition (PBII&D) [19–25].

In this work, samples coated by a standard CA process and by the PBII&D process, with and without nitriding as pre-treatment, were characterized. The effect of the various surface treatments on corrosion resistance was analyzed.

2. Experimental

Samples of 5 mm height were sliced from an AISI 316L stainless steel rod of 24 mm in diameter. The surface to be nitrided or coated

---

* Corresponding author. Tel.: +54 223 4816600x248; fax: +54 223 4810046.
E-mail addresses: lescalada@fi.mdp.edu.ar (L. Escalada), mail@johanna-lutz.de (J. Lutz), sonia@frcu.utn.edu.ar (S.P. Brühl), fazio@tinfip.lfp.uba.ar (M. Fazio), amarquez@df.uba.ar (A. Márquez), stephan.maendl@iom-leipzig.de (S. Mändl), darina.manova@iom-leipzig.de (D. Manova), ssimison@fi.mdp.edu.ar (S.N. Simison).

0257-8972/$ – see front matter © 2013 Elsevier B.V. All rights reserved.
http://dx.doi.org/10.1016/j.surfcoat.2013.02.025

was grinded and then polished with 1 μm diamond paste. The 316L stainless steel sample without treatment was considered as 'blank'.

The nitriding process was carried out in a DC pulsed plasma sustained with a mean voltage of 450 V, 500 Hz, duty factor 35%. The nitriding process was performed in a mixture of hydrogen and 23% nitrogen for 10 h and it was preceded by 2 h sputtering in Ar and H_2. During nitriding, the current density was kept at 0.1 mA/cm^2 and the temperature at 400 °C.

The coatings were deposited by a cathodic arc in an experimental device described elsewhere [22]. The standard CA TiN coating was achieved by running the discharge between a titanium cathode and the vacuum chamber acting as anode, with 130 A current. The sample was placed 20 cm away from the cathode and it was immersed in a nitrogen atmosphere with a continuous gas flux of 25 sccm and a working pressure in the range of $2–4 \times 10^2$ Pa. It was exposed to the arc during 2 min; the coatings were produced with two consecutive discharges. In the case of the PBII&D process, the same equipment was used but the sample was biased with negative pulses of 8 kV peak voltage, 70 μs pulse duration and a repetition rate of 200 Hz.

In order to infer the energy delivered by the ions that impinged on the surface during the coating process a calorimeter was placed on the chamber axis at the same distance from the cathode surface than the samples. The temperature change during the process was measured with a calorimeter, and the energy transferred per unit time by the impinged ions on the surface (Γ) was determined with a procedure described in ref. [26]. The calorimeter was composed of a thin Cu disk ~1 cm diameter and 0.1 cm thickness welded to the sheath of an ungrounded J-type thermocouple. The temperature change was measured by exposing the calorimeter to a 30 s discharge. The evolution of the temperature has been also registered for 30 min after the arc had been turned off, with the purpose of evaluating the heat loss of the measurement system. In the case of the discharge conditions for PBII&D, the pulse bias generator was connected to the thermocouple sheath.

After both processes, samples were transversally cut and included in resin and they were metallographically polished with 0.05 μm diamond paste. The structure of the nitrided layer was revealed using Marble reagent. The thickness and microstructure of the nitrided layer and the coating were analyzed by means of optical microscopy (Olympus PMG3), SEM equipped with Focus Ion Beam (FIB-SEM dual beam FEI Helios nanolab 600, 5 kV) and glancing angle XRD, at 2° incidence using Kα Cu radiation. Depth profiling of the samples was performed using secondary ion mass spectroscopy (SIMS) in a time-of-flight setup with 15 keV^{69}Ga + primary ions for a scanned area of 50×50 μm^2. Sputtering for depth profiling was performed with 2 keV oxygen ions. The secondary ion beam was scanned across 300×300 μm^2 to avoid crater edge effects.

Electrochemical experiments were conducted at room temperature and atmospheric pressure in a three-electrode cell. A saturated calomel electrode (SCE) was employed as the reference electrode and a platinum spiral wire as the counter electrode. So as to avoid altering ground surface, the samples were pressed against the bottom of the cell and sealed using an O-ring.

Corrosion resistance was evaluated by means of cyclic potentiodynamic polarization using a potentiostat VoltaLab PGZ 402. The potential was scanned at a sweep rate of 1 mV/s between the open circuit potential and E_{200}, the sweep reversal potential. This potential is arbitrarily chosen to attain a current density of 200 μA/cm^2 [27,28].

After the corrosion experiments, the surface morphology of the samples was examined using AFM (contact mode atomic force microscopy using an Agilent 5500 microscope), optical microscope and SEM (JEOL JSM-6460LV scanning electron microscope). Energy dispersive X-ray spectroscopy (EDS) analysis under SEM was employed to estimate the surface composition of different regions of the samples.

3. Results and discussion

3.1. Surface and coating structure and composition

After etching with Marble reactant, the nitrided samples showed a uniform "white layer" of 6–7 micron width. It is well known that for stainless steel this layer is a nitrogen expanded austenite phase free of nitride precipitates, called "S phase" or γ_N [2–5].

The X ray diffraction pattern shows the γ_N peaks shifted to lower angles and the γ peaks which come from the base material (Fig. 1a). In the coated sample (Fig. 1b), three characteristic TiN peaks are clearly observed at $2\theta = 42.6°$, 36.7° and 61.8°. The alpha peak comes possibly from a shallow martensitic structure formed during grinding and polishing before the coating. No evidence of nitride precipitation was found in the XRD spectra.

The TiN coatings over a nitrided sample are shown in Fig. 2, in a cross section after ion beam milling with the SEM equipped with FIB. The measured coating thicknesses were 280 nm for the CA coating in Fig. 2a and 510 nm for the PBDII&D coating (Fig. 2b). In both films a nodular surface topography structure can be observed, and a dense structure with columnar grains of less than 100 nm in width is also revealed in Fig. 2. The TiN films were deposited with two subsequent discharges, and a bilayer could be observed in both cases, CA and PBII&D coatings, indicating that the implantation did not change this structure.

In Fig. 3, SIMS profiles of the TiN coated samples with CA and PBII&D are shown. Assuming the film depth as the distance where

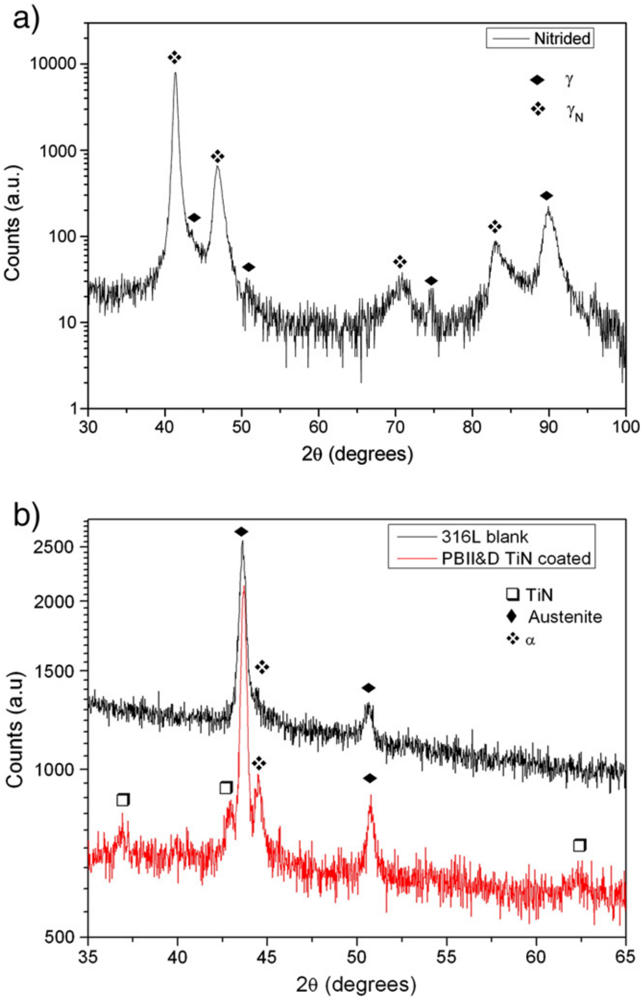

Fig. 1. GI XRD of (a) nitrided sample and (b) PBII&D TiN coated sample.

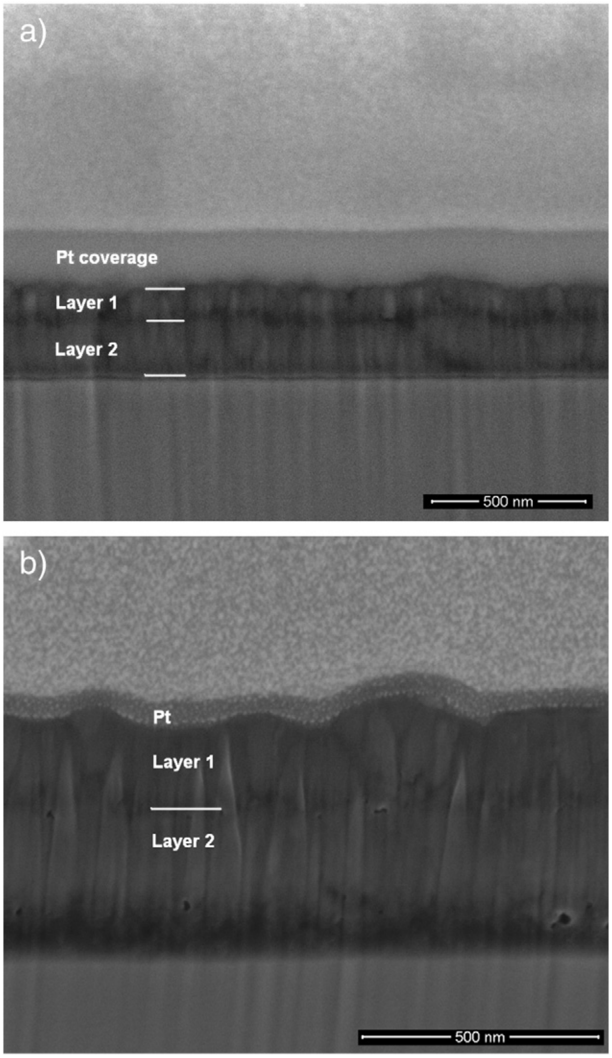

Fig. 2. SEM-FIB micrograph, scale corrected according 52° tilt: a) CA coating and b) PBII&D coating.

the Ti signal falls down, in the CA coating the film thickness is between 250 and 280 nm, and about 400 nm in the TiN film deposited by PBII&D. In both cases hydrogen within the film is a contamination from the coating process and the O signal is a consequence of the oxygen sputtering. The region with enhanced Ti and N count rate inside the substrate can be defined as interface, specifically the region between 80% and 20% of the Ti signal, considering the maximum value as 100%. The interface is 50% thicker in the case of the PBII&D due to ion implantation. The implantation process not only makes possible an intermixing in the surface layer but also changes the diffusion profile, mainly because of the thermal energy delivered by the impinging ions [19].

The SIMS analysis of the duplex PBII&D – implantation and deposition over nitride samples – is presented in Fig. 4. It can be observed that the composition of the film is similar to the ones on the previous non-nitrided and coated samples (Fig. 3). The film of the duplex PBII&D is as thick as the PBII&D coating on non-nitrided 316L but the interface is thicker. In Fig. 4b, the nitride layer, resulting from the nitriding process, can be observed underneath the TiN coating. As the ionization rate for nitrogen is quite low, the nitrogen content has to be obtained from comparisons with calibrated standards, yielding about 50 at.% within the TiN and 30–35 at.% near the surface of the nitrided steel.

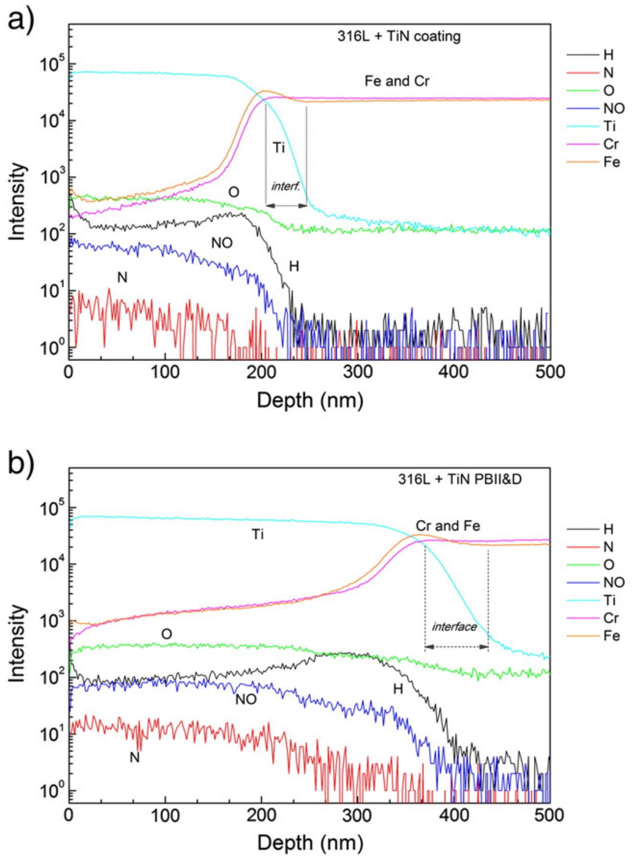

Fig. 3. SIMS composition depth profile of: a) sample coated with CA TiN and b) sample coated with PBII&D TiN.

The increase of the growth rate of TiN films when a high voltage bias pulse was applied has been also reported with other PBII&D devices [20,24,29]. This behavior can be attributed to an increase of the adatom sticking promoted by the energy delivered to the surface through the accelerated ions impinging, even though the sputtering rate is also increased with the bias.

The temperature variations registered after a 30 s discharge were ~270 °C without bias and ~650 °C when the pulsed bias was applied. Considering the heat loss of the calorimeter system, the Γ found values were ~2.0 J/s and 5.4 J/s, respectively. Some calculation and modeling of the energy released in these processes and the sputtering rates are presented in the following paragraphs, in order to explain the difference in thickness in the coatings with and without implantation, CA and PBII&D.

Γ can be related to plasma parameters as follows [26]:

$$\Gamma = (2/m_i)^{1/2} n_i z^{3/2} {E_i*}^{3/2} A \tag{1}$$

where n_i is the ion density, m_i the ion mass, E_i*is the kinetic energy per unit charge of the ions arriving to the Cu disk, z is the average ion charge and A the calorimeter area. While bias is off, ions arrive to the surface with the same kinetic energy with which they were ejected from the cathode region (E_{i0}), because energy losses by collisions with neutral particles are negligible at the working pressure. Considering typical values reported for titanium vacuum arcs, without bias $E_i^* = E_{i0} = 40$ eV and $z = 1.8$ [30], and from the Γ value experimentally determined without bias, n_i was estimated as ~1×10^{17} m^{-3}. When bias is on, ions are accelerated by the voltage pulse of amplitude $-V_0$. In the time scale that takes the transient plasma sheath to evolve towards a steady-state (τ), the energy

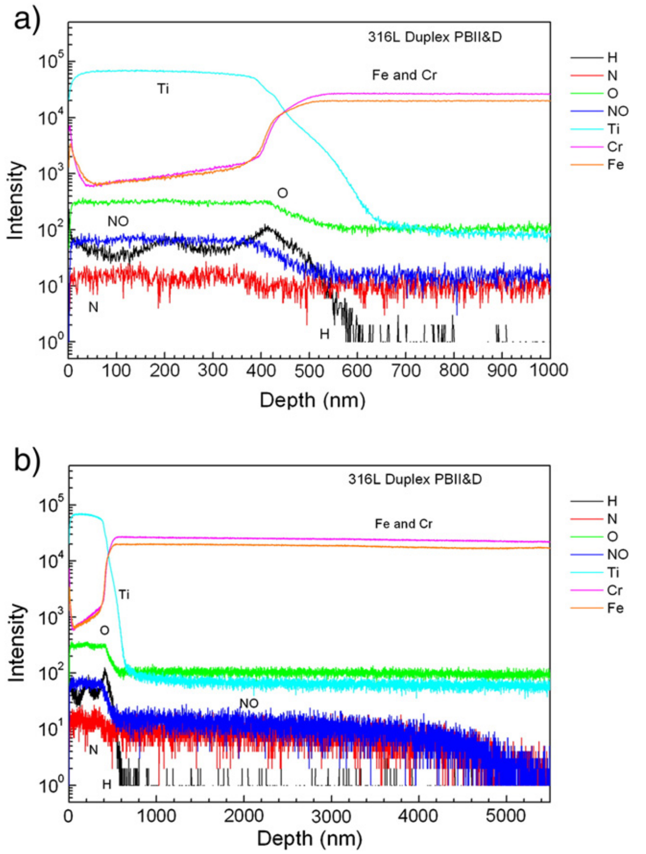

Fig. 4. SIMS of the sample nitrided and coated with TiN by PBII&D; a) near surface profile and b) the whole depth profile.

acquired by the accelerated ions per unit charge is ~eV_0. The time τ corresponding to the establishment of a steady-state Child law sheath is [31]

$$\tau{\sim}\left(\sqrt{2/_9}\right)\omega_{pi}^{-1}\left({}^{2zV}\!\big/_{Te}\right)^{3/4} \tag{2}$$

being $\omega_{\rm pi}$ the ion plasma frequency and T_e the electron temperature. Thus, the average kinetic energy delivered by the ions can be approximated as

$$E_i^* = {}^{i}eV_0\tau/T + E_{i0}(l-\tau/T) \tag{3}$$

where T is the pulse duration. Typical T_e values reported for titanium vacuum arcs are in the range of 1–5 eV, taking an intermediate value for T_e and the n_i value determined above, τ results ~ 2 μs. Replacing in Eq. (1) the value of E_i* derived from Eq. (3) with the parameters of the experiment ($V_0 = 8$ kV, $T = 5 \times 10^{-3}$ s) and $\tau = 2\,\mu$s, Γ can be calculated and the value agrees with the measured one with the calorimeter for the PBII&D process, which validates this experimental determination of the energy released by the ions in the process with pulsed bias.

A rough estimation of the temperature achieved on the substrate surface due to the exposure of the sample to the discharge can be obtained solving the heat conduction equation for semi-infinite, one dimensional solid with a uniform heat flux determined from Γ [31]. For a 2 min discharge the surface temperature was estimated in the order of 50 °C without bias and of 150 º C with the pulse bias applied. This surface heating as a consequence of the energy delivered by the ions can increase significantly the deposition rate, according to results reported for TiN films deposited with a cathodic arc on steel [32]. Additionally, the sputter yields of Ti and N atoms produced by Ti^{2+} incident ions on TiN have been obtained from the SRIM code [33]. The total sputter yield values at 80 eV and at 16 keV are 0.15 and 2.9 atom/ion, respectively. Therefore, the sputtering can be neglected while the pulse is off and must be considered when the pulse is on, but only during the effective time of ion acceleration τ. The deposition rate (η) is related to the ion particle flux arriving at the surface and the sputtered atoms through

$$\eta = an_i(2\,zE_{i0}/m_i)^{1/2}(m_{TiN}/r_{TiN})(1-\tau/T) - yn_i(2\,z\,eV_0/m_i)^{1/2}(m_{TiN}/r_{TiN})\tau/T \tag{4}$$

where ρ_{TiN} and $m_{\rm TiN}$ are the TiN bulk density and molecular mass, respectively, a is the sticking coefficient and y the total sputter yield. From the experimental results, η was calculated approximately as 70 nm/min for the process without bias (CA coating) and 120 nm/min for the PBII&D process, and then, the corresponding a values result in 0.03 and 0.08, respectively. Here is a factor 2 between without bias and with bias but they are very low values, and it can be concluded that the increase in the sticking coefficient can be only justified with the difference found in the surface temperatures.

3.2. Corrosion tests

3.2.1. Cyclic polarization curves of CA TiN coated, nitrided and duplex samples

The effect of the nitrided layer as pre-treatment in the corrosion behavior of a CA TiN coating was analyzed. From the polarization curves (Fig. 5), it can be observed that the nitrided layer had better corrosion behavior than the blank, having a far nobler reversal potential and lower anodic currents.

The blank AISI 316L sample suffered pitting corrosion, as usual for this steel in chloride media. On the contrary, in the nitrided steel, no visible pits but a great amount of colored spots appeared on the tested surface when observed with the optical microscope (Fig. 6a). The same occurred in the CA TiN coated, showed in Fig. 6b. These spots could not be detected by SEM observation, indicating that the corrosion attack was very shallow and there was no detectable change of surface topography. AFM surface evaluation of a nitrided sample indicated that these spots were in fact little pits with a mean depth of 0.5 μm and that they were surrounded by some corrosion products with less than 100 nm thickness, as it can be observed in Fig. 6c.

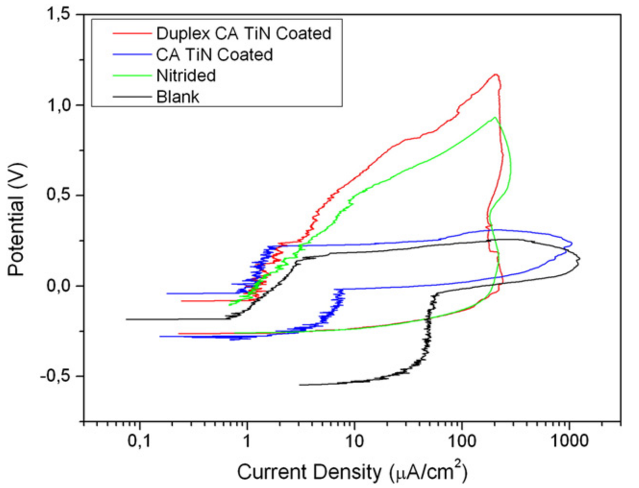

Fig. 5. Cyclic polarization curves of nitrided 316L steel, with and without TiN coating.

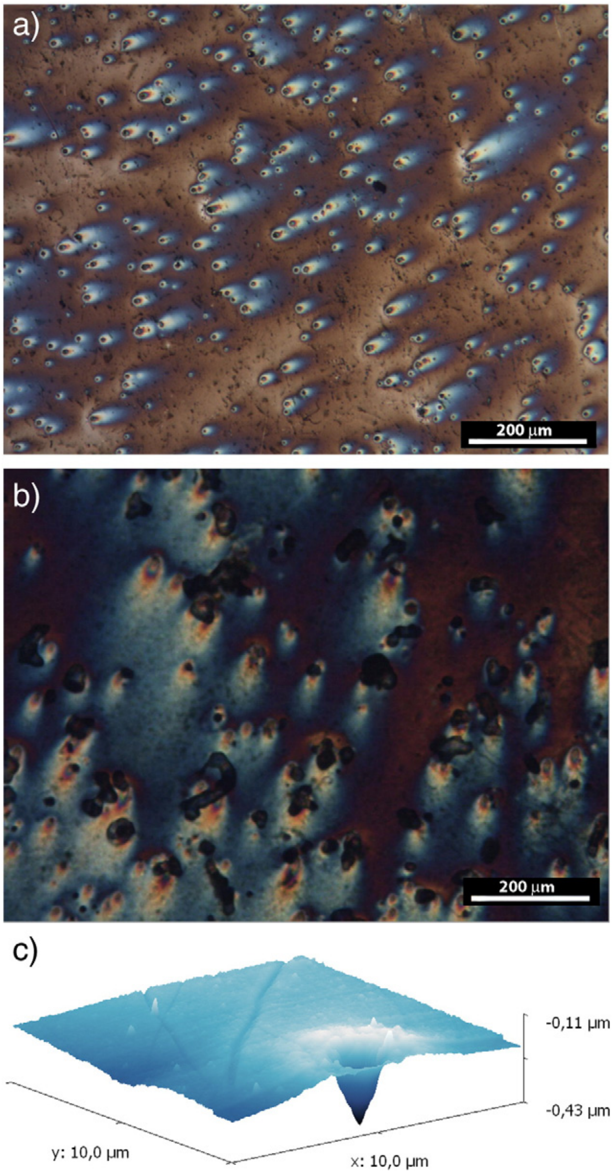

Fig. 6. Optical microscopy of the morphology of the attack. a) Nitrided sample, b) nitrided and CA coated sample, c) 3D graph of one pit in the nitrided sample, from the topographic view with AFM.

It can also be demonstrated from the curves in Fig. 5 that the coating itself has little effect onto the blank material corrosion resistance. The value of the maximum potential does not differ very much from that of the blank sample. In this case, the attack was localized under the o-ring in the form of crevice corrosion. The CA TiN film is very hard compared with the 316L substrate and several initiation sites for crevice corrosion may be created if the film is fractured, in the place where the o-ring is pressed onto the substrate.

The major improvement on the localized corrosion resistance is observed when the coating is deposited onto the nitrided layer. The potential at which the current density reaches the value of 200 μA/cm^2 (E_{200}) is 600 mV nobler than the one corresponding to the blank samples.

By microscopic examination of the CA coated sample it was observed, that the film was detached around the attacked zone, showing that the adhesion was not very good. On the contrary, in the case of the duplex sample, no detachment was observed, indicating that the nitrided layer is adequate as a pre-treatment for a TiN film, not only providing a mechanical support but also giving a better corrosion resistance than the blank material.

In order to determine the effect of corrosion on the coating composition, the samples were analyzed by means of SEM and EDS, comparing the zones affected by the corrosion test and the non-corroded one. Out of the corroded zone, the presence of nitrogen and titanium was detected by EDS and also the signals of the substrate composition. After the polarization test the EDS analysis of the corroded zone showed that the coating kept its composition without any detectable change (within the limits of this technique).

3.2.2. Analysis of CA and PBII&D TiN coating, with nitriding as pre-treatment

The effect of ion implantation in the localized corrosion resistance is shown in Fig. 7. For comparison, the PBII&D duplex treatment is shown together with the CA duplex treated sample and the nitrided sample.

It is observed that both duplex processes provide a beneficial effect on corrosion resistance, since E_{200} potentials are higher than those of the nitrided sample without coating. This indicates a higher resistance to film breakdown and to localized corrosion attack. Besides anodic currents are lower, so the dissolution rate is diminished.

It can be observed that the coating with implantation (PBII&D) leads to the best corrosion resistance. Although E_{200} is 70 mV lower than in the CA coated, the current density values were between 2 and 3 times lower for the same voltage value almost throughout the whole test. The very good corrosion behavior is mainly attributed to the higher thickness of the PBII&D coating, the wider interlayer and its structure, where the intermixing created by implantation (Fig. 4) seemed to produce a more protective thin film.

The corroded surface of the PBII&D duplex samples was observed with SEM (Fig. 8a) and optical microscope (Fig. 8b). The same little spots surrounded by colored zones which were observed by optical microscopy in the nitrided samples (Fig. 6) were formed here, indicating that once the film was detached, the corrosion process was the same. Besides, no pitting or crevice attack could be detected. EDS spectra were similar in the corroded and non-corroded zones but some detachment of the coating was observed in certain zones.

As a summary of the corrosion tests, when corrosion was enhanced by a high anodic potential, both coatings failed because of film delamination, and some shallow pits were produced. Nevertheless, the combination of nitriding and the PBII&D coating demonstrated to be the best system because current density values were the smallest. This improvement could be related to a better coverage of the surface (less surface exposure or/and less defective film) enhanced by the intermixing implantation. Considering that PVD films are hardly free of defects, the duplex structure obtained with this coating technique on top of a corrosion resistant nitrided layer could be a good alternative for the operation in aggressive environments.

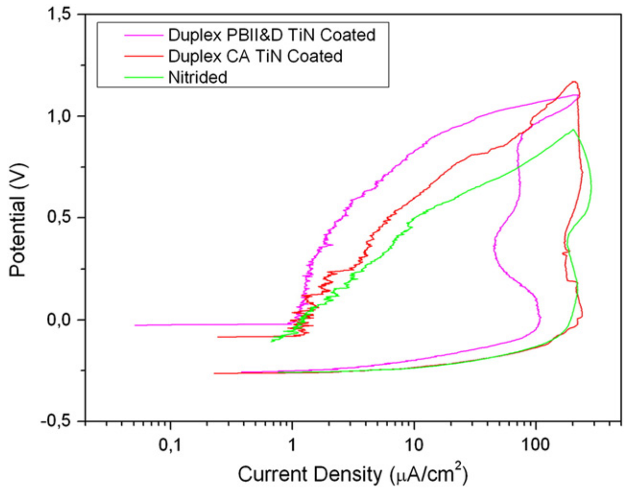

Fig. 7. Cyclic polarization curves nitrided and duplex treated 316L steel.

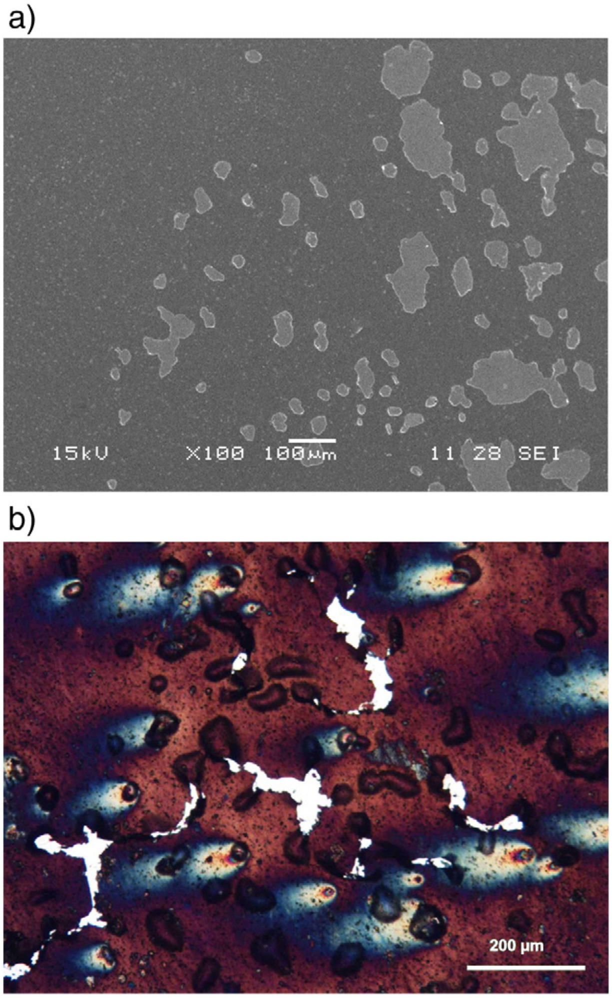

Fig. 8. Duplex PBII&D sample: a) SEM observation of the border of the tested zone and b) optical micrograph of the same zone.

4. Conclusions

Four surface treatments were investigated: (i) CA TiN coating over non-nitrided and (ii) CA TiN coating over nitrided steel, (iii) PBII&D coating over nonnitrided steel and (iv) PBII&D coating over nitrided steel.

The first case – the CA TiN coating on non-treated steel (i) – resulted in no appreciable enhancement in the resistance to localized corrosion. On the other hand, the addition of a previous nitriding treatment (ii) improved the corrosion behavior which was even further enhanced in the case of the PBII&D treatments (iv). The plasma based ion implantation and deposition (PBII&D) duplex treatment had the best corrosion resistance of the four systems investigated in a 3.5% NaCl solution, far better than that of AISI 316L itself.

This good behavior could be attributed to the presence of a suitable mechanic interlayer on top of the soft base material, consisting of a 6–7 μm nitrided layer (“S-phase”), obtained at low temperature and low nitrogen content (390 °C, 23 at.% nitrogen). This nitriding pre-treatment proved to be resistant to localized corrosion, while the deposition of the TiN film with ion implantation yielded a compact film, and also produced an intermixing between the coating and the nitrided layer which resulted in a better coating adhesion and hence a higher protection against localized corrosion under the conditions tested.

The higher deposition rates of TiN coatings obtained by PBII&D respect to that deposited by CA can be associated to the increase of the surface temperature promoted by the energy delivered to the surface through the accelerated ions impinging. This effect would produce an increase of the adatom sticking enough not only to compensate the sputtering rate but also to duplicate the deposition rate. In the future, the influence of some coating parameters, such as ion flux, temperature and nitrogen flow, should be analyzed to study their influence in mechanical properties (adhesion, load bearing capacity) which could lead to an even better corrosion resistance.

Acknowledgments

The authors would like to acknowledge the financial supports from the following agencies: Universidad Tecnológica Nacional (Project 25/D046), CONICET (PIP 11220090100219), ANPCyT (PICT 1807), Program of Scientific and Technological Cooperation between Ministerio de Ciencia, Tecnología e Innovación Productiva of Argentina (MINCYT, Project Code AL/09/03) and Bundesministerium für Bildung und Forschung (BMBF, Project Code ARG 09/006) of Germany.

References

[1] L. Escalada, J. Lutz, S. Mändl, D. Manova, H. Neumann, S. Simison, Surf. Coat. Technol. 211 (2012) 76.
[2] N. Mingolo, A.P. Tschiptschin, C.E. Pinedo, Surf. Coat. Technol. 201 (2006) 4215.
[3] L. Gil, S. Brühl, L. Jiménez, O. Leon, R. Guevara, M.H. Staia, Surf. Coat. Technol. 202 (2008) 1802.
[4] X. Li, T. Bell, Corros. Sci. 46 (2008) 1527.
[5] D. Manova, G. Thorwarth, S. Mändl, H. Neumann, B. Stritzker, B. Rauschenbach, Nucl. Instr. Meth. B 242 (2006) 285.
[6] L. Nosei, M. Avalos, B.J. Gómez, L. Nachez, J. Feugeas, Thin Solid Films 468 (2004) 134.
[7] A. Fossati, F. Borgioli, E. Galvanetto, T. Bacci, Corros. Sci. 48 (2006) 1513.
[8] L.C. Gontijo, R. Machado, E.J. Miola, L.C. Casteletti, N.G. Alcântara, P.A.P. Nascente, Mater. Sci. Eng. 431 (2006) 315.
[9] K.L. Choy, Prog. Mater. Sci. 48 (2003) 57.
[10] R.J. Rodríguez, J.A. García, A. Medrano, M. Rico, R. Sánchez, R. Martínez, C. Labrugère, M. Lahaye, A. Guette, Vacuum 67 (2002) 559.
[11] E.S. Puchi-Cabrera, F. Martínez, I. Herrera, J.A. Berríos, S. Dixit, D. Bhat, Surf. Coat. Technol. 182 (2004) 276.
[12] A. Matthews, A. Leyland, A. Wilson, Vacuum 68 (2002) 57.
[13] J. Smolik, J. Walkowicz, J. Tacikowski, Surf. Coat. Technol. 125 (2000) 134.
[14] H. Dong, Y. Sun, T. Bell, Surf. Coat. Technol. 90 (1997) 91.
[15] W. Wu, X. Li, J. Chen, H. Dong, Surf. Coat. Technol. 203 (2009) 1273.
[16] K.T. Short, Z. Zhang, K. Finnie, G.A. Collins, C.A. Figueroa, Mater. Lett. 62 (2008) 3156.
[17] C. Liu, G. Lin, D. Yang, M. Qi, Surf. Coat. Technol. 200 (2006) 4011.
[18] L. Chenglong, Y. Dazhi, L. Guoqiang, Q. Min, Mater. Lett. 59 (2005) 3813.
[19] A. Anders, Surf. Coat. Technol. 183 (2004) 301.
[20] M.M. Bilek, D.R. McKenzie, R.N. Tarrant, S.H.M. Lim, D.G. McCulloch, Surf. Coat. Technol. 156 (2002) 136.
[21] W. Attenberger, G. Thorwarth, D. Manova, S. Mändl, B. Strizker, B. Rauschenbach, Surf. Coat. Technol. 142–144 (2004) 412.
[22] A. Arias Duran, M. Fazio, A. Kleiman, L. Giuliani, A. Márquez, D. Grondona. Study of the efficiency of magnetic island macroparticle filters for different vacuum arc configurations. Journal of Physics: Conference Series 370 (2012) 012016.
[23] S.H.N. Lim, D.G. McCulloch, S. Russo, M.M.M. Bilek, D.R. McKenzie, Nucl. Instr. Meth. B 190 (2002) 723.
[24] P. Huber, D. Manova, S. Mändl, B. Rauschenbach, Surf. Coat. Technol. 174–175 (2003) 1243.
[25] G.J. Wan, N. Huang, Y.X. Leng, P. Yang, J.Y. Chen, J. Wang, H. Sun, Surf. Coat. Technol. 186 (2004) 136.
[26] H. Kelly, F.A. Lepone, A. Márquez, J. Appl. Phys. 89 (2001) 1567.
[27] A.D. Sosa, M.D. Echeverría, O.J. Moncada, S.N. Simison, Mater. Lett. 62 (2008) 100.
[28] S.P. Brühl, R. Charadia, S. Simison, D.G. Lamas, A. Cabo, Surf. Coat. Technol. 204 (2010) 3280.
[29] W. Yongqiang, Ch. Xiaoxia, T. Xiubo, G. Chunzhi, Y. Shiqin, J. Zhiqiang, Ch. Liangji, Vacuum 89 (2013) 185.
[30] In: R.L. Boxman, D.M. Sanders, P.J. Martin (Eds.), Handbook of Vacuum Arc Science and Technology, Fundamentals and Applications, Noyes, Park Ridge, NJ, 1995.
[31] In: A. Anders (Ed.), Handbook of Plasma Immersion Ion Implantation and Deposition, Wiley-VCH, Weinheim, 2004, p. 243.
[32] R. Vieira, M.C.A. Nono, Mater. Sci. Forum 498–499 (2005) 717.
[33] J.F. Ziegler, http://www.srim.org.